

# Continuous measurements of two qubits

Wenjin Mao and Dmitri V. Averin

*Department of Physics and Astronomy, Stony Brook University, SUNY, Stony Brook, NY 11794-3800*

Francesco Plastina

*Dipartimento di Fisica, Universita' della Calabria, I-87036 Arcavacata di Rende (CS), Italy*

Rosario Fazio

*NEST-INFM & Scuola Normale Superiore, 56126 Pisa, Italy*

(November 14, 2018)

We develop a theory of coherent quantum oscillations in two, in general interacting, qubits measured continuously by a mesoscopic detector with arbitrary non-linearity and discuss an example of SQUID magnetometer that can operate as such a detector. Calculated spectra of the detector output show that the detector non-linearity should lead to mixing of the oscillations of the two qubits. For non-interacting qubits oscillating with frequencies  $\Omega_1$  and  $\Omega_2$ , the mixing manifests itself as spectral peaks at the combination frequencies  $\Omega_1 \pm \Omega_2$ . Additional nonlinearity introduced by the qubit-qubit interaction shifts all the frequencies. In particular, for identical qubits, the interaction splits coherent superposition of the single-qubit peaks at  $\Omega_1 = \Omega_2$ . Quantum mechanics of the measurement imposes limitations on the height of the spectral peaks.

## I. INTRODUCTION

Quantum measurements represent an important part of quantum information processing, quantum computing, and evolution of quantum systems in general. Counter-intuitive features of the measurement process related to the collapse of the wave-function of the measured system continue to attract interest to the “problem of quantum measurements”. Physics of mesoscopic solid-state qubits and detectors provides convenient tools for studying this problem in the most interesting case of quantum systems that are large on atomic scale – see, e.g., chapters on quantum measurements in<sup>1</sup>. Many features of quantum measurements manifest themselves directly in the regime of “continuous” measurements in which the measured system evolves in time being continuously affected by the detector back-action which implements the wave-function collapse dynamically. Simple example of this regime is provided by the linear weak measurements of coherent quantum oscillations in one qubit<sup>2–6</sup> which have been demonstrated experimentally in<sup>7</sup>. An interesting property of the continuous weak measurements is that the spectrum of the detector output has features that characterize directly the quantum mechanics of measurement and quantum nature of the qubit oscillations.

One of the suggested tools in quantum-information applications of quantum measurements are quadratic measurements, realized when the detector response to the input signal is quadratic. Quadratic measurements should make it possible to monitor products of operators of different quantum systems, and can be used, for instance, to implement simple schemes of error-correction<sup>8</sup>, or to entangle non-interacting qubits<sup>9</sup>. The purpose of our work is to study the regime of continuous quadratic measurements concentrating on the case of two qubits which is

the simplest system that reveals non-trivial characteristics of quadratic measurements. Currently, systems of two coupled mesoscopic qubits are almost routinely studied in experiments – see<sup>10–14</sup>. As discussed in this work, for two qubits, quadratic measurements are equivalent to measurements with arbitrary nonlinearity. Qualitatively, the main feature of continuous non-linear measurements is the mixing of coherent oscillations in individual qubits that for non-interacting qubits leads to appearance of spectral peaks at combination frequencies  $\Omega_1 \pm \Omega_2$ , where  $\Omega_j$  are the frequencies of individual oscillations. In contrast to mixing of classical oscillations, only these two combination frequencies appear in the detector output, and as in the linear regime, intensity of all spectral peaks is limited by the quantum mechanics of measurement.

The paper is organized as follows. Section II introduces a model of mesoscopic solid-state detectors used in this work and gives an explicit description of one practical detector which realizes this model and can operate in the purely quadratic or non-linear regime. Section III describes the two-qubit system and derives explicit equations for the evolution of the density matrix of this system in the measurement process. In Section IV we use these equations to calculate output spectral density of the non-linear detector measuring the two-qubit system in several situations. Section V provides concluding remarks.

## II. MESOSCOPIC QUANTUM MEASUREMENTS

In this Section, we describe a generic model of quantum measurements with a mesoscopic solid-state detector and provide a detailed discussion of one specific example of such a detector.

### A. General model of a mesoscopic detector

Although mesoscopic detectors can have quite different physical implementations and include, e.g., quantum point contacts (QPC)<sup>15–17,19–22</sup>, normal and superconducting SET transistors<sup>23–29</sup>, SQUID magnetometers<sup>30</sup> and generic mesoscopic conductors<sup>31,32</sup>, the operating principle of all these detectors is essentially the same. Measured quantum system controls, through an operator  $x$ , the transmission amplitude  $\hat{t}(x)$  of particles (they can be electrons, Cooper pairs, or magnetic flux quanta) between the two reservoirs. The flux of these particles provides then the information on the state of this system. Schematics of the detector of this type measuring two qubits is shown in Fig. 1.

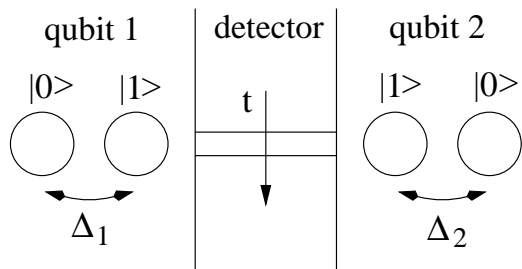


FIG. 1. Diagram of a mesoscopic detector measuring two qubits. The qubits modulate amplitude  $t$  of tunneling of detector particles between the two reservoirs.

Quantitatively, the Hamiltonian of the detector-system coupling for such a detector consists of detector tunneling modulated by the measured system and can be written as

$$H_T = \hat{t}(x)\xi + \hat{t}^\dagger(x)\xi^\dagger, \quad (1)$$

where  $\xi, \xi^\dagger$  are the detector operators that create excitations when a particle is transferred, respectively, forward and backward between the reservoirs. For the quantum-point-contact (QPC) detector, which represents the simplest realization of the model discussed in this Section,  $\xi, \xi^\dagger$  describe excitation of electron-hole pairs in the QPC electrodes.

We make several additional assumptions about the detector. We suppose that the tunneling between the detector reservoirs is weak and can be accounted for in the lowest non-vanishing order in the tunneling Hamiltonian (1). Under this assumption, the precise form of the internal detector Hamiltonian  $H_d$  is not important and dynamics of measurement is defined by the correlators:

$$\gamma_+ = \int_0^\infty dt \langle \xi(t)\xi^\dagger \rangle, \quad \gamma_- = \int_0^\infty dt \langle \xi^\dagger(t)\xi \rangle, \quad (2)$$

where the angled brackets denote averaging over the detector reservoirs which are taken to be in a stationary state with the density matrix  $\rho_D$ :  $\langle \dots \rangle = \text{Tr}_D \{ \dots \rho_D \}$ . The correlators (2) set the scale  $\Gamma_\pm \equiv 2\text{Re}\gamma_\pm$  of the forward and backward detector tunneling rates. The correlators  $\langle \xi(t)\xi \rangle$ ,  $\langle \xi^\dagger(t)\xi^\dagger \rangle$  that do not conserve the number

of tunneling particles are assumed to vanish. As can be seen more explicitly from the example of the SQUID detector discussed below, this condition holds even in the case of superconducting detectors, where such “anomalous” correlators can exist in general. Under the condition of large bias voltage important in our model of the detector operation, the Cooper-pair tunneling is incoherent, and anomalous correlators indeed vanish.

Another assumption is that the characteristic time of the detector tunneling is much shorter than that of the evolution of the measured system. One of the conditions implied by this assumption is that the energy bias  $\Delta E$  for tunneling through the detector, which sets one of the tunneling time scales,  $\Delta E^{-1}$ , is much larger than the typical energies  $E_0$  of the measured system. In the example of the QPC detector,  $\Delta E = eV$ , and this condition means that the bias voltage  $V$  across the QPC is sufficiently large. For short tunneling times, the functions  $\xi(t)$ ,  $\xi^\dagger(t)$  in Eq. (2) are effectively  $\delta$ -correlated on the time scale of the dynamics of the measured system. Condition of the large energy bias  $\Delta E$  for the detector tunneling leading to the correlators Eq. (2) being  $\delta$ -correlated is the natural part of the measurement model: it enables one to neglect quantum fluctuations in the detector in the frequency range that corresponds to that of the measured system, and makes the detector response in this frequency range classical.

Combined with the assumption of weak tunneling, vanishing correlation time in the correlators (2) makes it possible to write down simple evolution equations for the density matrix  $\rho$  of the measured system. Indeed, the time evolution of  $\rho$  in the interaction representation with respect to the tunneling Hamiltonian (1) is given by the standard expression:

$$\rho(t) = \text{Tr}_D \{ S \rho_D S^\dagger \}, \quad S = T \exp \left\{ -i \int_0^t dt' H_T(t') \right\}. \quad (3)$$

If the detector operators in Eq. (2) are  $\delta$ -correlated, one can keep only the “non-crossing diagrams” in the perturbation expansion of Eq. (3) in  $H_T$ . Evolution of  $\rho(t)$  in Eq. (3) is governed then by the following equation:

$$\begin{aligned} \dot{\rho} = & \Gamma_+ \hat{t}^\dagger \rho \hat{t} + \Gamma_- \hat{t} \rho \hat{t}^\dagger - (\gamma_+ \hat{t} \hat{t}^\dagger + \gamma_- \hat{t}^\dagger \hat{t}) \rho - \\ & \rho (\gamma_+^* \hat{t} \hat{t}^\dagger + \gamma_-^* \hat{t}^\dagger \hat{t}). \end{aligned} \quad (4)$$

Equation (4) describes the measurement-induced part of the evolution of an arbitrary measured system within our generic model of a mesoscopic detector.

One general remark that should be made here is that for some detectors, e.g. SET transistors, there are regimes of operation, when the particle transfer through the detector consists of more than one steps and can not be characterized by one transmission amplitude. Our measurement model is not applicable in these regimes. We focus on the case of one-step transfer, however, since

only in this case the detector can be quantum-limited: intermediate steps introduce additional back-action dephasing for the measured system without increasing information contained in the detector tunneling rate.

Evolution (4) of the density matrix  $\rho$  of the measured system is reflected in the detector output: the particle current between the detector reservoirs. Using the same logic that lead to Eq. (4), one can see that the assumed large difference between the time scale of detector tunneling and evolution of the measured system makes it possible to reduce the expression for the particle current to the form of the operator  $I$  in the space of the measured system:

$$I = (\Gamma_+ - \Gamma_-)t^\dagger t. \quad (5)$$

This equation gives both the dc current

$$\langle I \rangle = \text{Tr}\{I\rho_0\}, \quad (6)$$

where  $\rho_0$  is the stationary solution of Eq. (4), and the current spectral density

$$S_I = S_0 + 2 \int_0^\infty d\tau \cos \omega \tau (\text{Tr}\{I e^{L\tau} [I\rho_0]\} - \langle I \rangle^2). \quad (7)$$

Here  $S_0$  represents the usual noise (typically, a mixture of shot and thermal noise) associated with tunneling:

$$S_0 = (\Gamma_+ + \Gamma_-) \text{Tr}\{t^\dagger t \rho_0\}, \quad (8)$$

and  $e^{L\tau}[A]$  denotes the evolution of the matrix  $A$  during time interval  $\tau$  governed by Eq. (4).

## B. DC SQUID as the non-linear detector

Before discussing applications of our measurement model that is expressed quantitatively by Eqs. (4)–(8), we give one explicit example of the mesoscopic detector (different from the simplest QPC detector that was already mentioned several times in this Section) that realizes this model. The detector is the strongly-biased dc SQUID shown schematically in Fig. 2. It consists of two Josephson junctions with critical currents  $I_{1,2}$  that are included in small superconducting loop shunted by a resistor with some impedance  $Z(\omega)$ , assumed to be featureless,  $Z(\omega) = Z(0) \equiv R$ , at low frequencies of variations of the measured magnetic flux  $\Phi$  through the SQUID loop. When the loop inductance is small, the difference between the two Josephson phases  $\varphi_{1,2}$  across the two junctions is directly linked to  $\Phi$ :

$$\varphi_1 - \varphi_2 = 2\pi\Phi/\Phi_0 \equiv \phi,$$

where  $\Phi_0 = \pi\hbar/e$  is the magnetic flux quantum. In this regime, the SQUID is equivalent to a single Josephson junction, with the effective amplitude of Cooper-pair tunneling controlled by the flux  $\Phi$ . Due to interference of the

Cooper-pair tunneling in the two SQUID junctions, the total tunneling amplitude is equal to the sum of tunneling amplitudes in the two Josephson junctions, with the amplitude in each junction being proportional to its critical current  $I_j$ . The total amplitude can then be written as

$$t(\phi) = i_1 e^{i\phi/2} + i_2 e^{-i\phi/2}, \quad (9)$$

where  $i_1 = (I_1/I_2)^{1/2}$  and  $i_2 = 1/i_1$  characterize the asymmetry of the two junctions.

The operating principle of the SQUID as a detector coincides with the one discussed in the beginning of this Section: variations of the flux  $\phi$  around some bias point  $\bar{\phi}$  lead to variations of the Cooper-pair tunneling amplitude (9) affecting the transfer rate  $I$  of Cooper pairs through the SQUID. Cooper-pair tunneling rate is reflected in the detector output: deviations  $V$  of the voltage across the SQUID,  $V = -2eIR$ , from the value  $V_0 = RI_0$  induced by the dc current bias  $I_0$  (see Fig. 2). An important feature of the SQUID detector is that in the case of identical junctions:  $i_1 = i_2 = 1$ , at the bias points when  $\bar{\phi}/2\pi$  is integer, the tunneling amplitude  $t(\phi)$  (9) varies quadratically as a function of  $\phi$ , with vanishing coefficient of the linear response. As shown explicitly in the next Section, under this bias condition the SQUID can act as the purely quadratic detector.

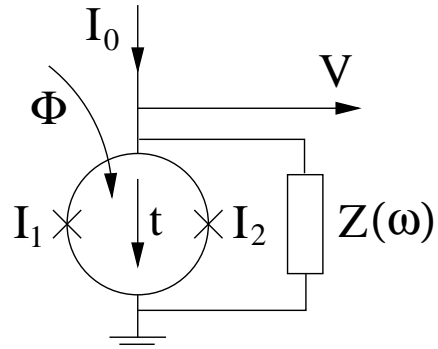


FIG. 2. DC SQUID detector formed by two Josephson junctions with critical currents  $I_{1,2}$  in a small superconducting loop shunted by the impedance  $Z(\omega)$ . The SQUID is biased by the dc current  $I_0$ , the voltage  $V$  is the measurement output and reflects the variations in the rate of incoherent Cooper-pair transfer through the SQUID with amplitude  $t$  controlled by the flux  $\Phi$ . Existence of the two interfering contributions to the tunneling amplitudes makes it possible for the SQUID to operate as a quadratic detector.

The Cooper-pair tunneling Hamiltonian in the SQUID can be expressed through the tunneling amplitude (9) similarly to Eq. (1):

$$H_T = -\frac{(I_1 I_2)^{1/2}}{4e} [t(\phi) e^{i(2eV_0 t + \varphi(t))} + \hat{t}^\dagger(\phi) e^{-i(2eV_0 t + \varphi(t))}], \quad (10)$$

where  $\varphi(t) = (\varphi_1(t) + \varphi_2(t))/2$  is the average Josephson phase across the SQUID which includes fluctuating

component accumulated due to the equilibrium voltage fluctuations across the impedance  $Z(\omega)$ . The fluctuations couple the Cooper-pair tunneling to  $Z(\omega)$  so that the transfer of a Cooper pair across the SQUID creates electromagnetic excitations in this impedance, the process described by operators  $e^{\pm i\varphi(t)}$  in Eq. (10). In this way, impedance  $Z(\omega)$  provides dissipation necessary to make the Cooper-pair transfer irreversible.

When the dc bias current  $I_0$  and associated voltage  $V_0 = RI_0$  across the dc SQUID are sufficiently large, one can treat the tunnel Hamiltonian (10) as perturbation (i.e., the dc current through the SQUID is much smaller than the bias current  $I_0$ ) and the system dynamics at low frequencies can be described as incoherent tunneling of Cooper pairs through the SQUID<sup>33</sup>. This regime satisfies both of the conditions on the detector dynamics discussed in the general detector model, and when the control flux  $\phi$  is created by the measured quantum system, measurement dynamics is governed by the same general equation for the system density matrix (4), where the correlators (2) are now given by the following expressions<sup>33</sup>:

$$\gamma_{\pm} = \frac{I_1 I_2}{16e^2} \int_0^{\infty} dt e^{\pm i2eV_0 t} \exp\left\{ \int \frac{d\omega}{\omega} \frac{\text{Re}Z(\omega)}{R_Q} \frac{e^{-i\omega t} - 1}{1 - e^{-\omega/T}} \right\}. \quad (11)$$

Here  $R_Q \equiv \pi\hbar/4e^2$  is the “quantum resistance”. Under the conditions of weak linear coupling of the SQUID detector to the measured systems, the correlators (11) that give the rates of incoherent Cooper-pair tunneling are the only relevant properties of the SQUID operating as a linear quantum detector<sup>4</sup>. If the variations of the external flux  $\phi$  controlling Cooper-pair tunneling are not small, the SQUID can act as non-linear, and in particular, purely quadratic detector. Dynamics of the measured system is reflected in the Cooper-pair current in the SQUID in exactly the same way as in the general model [see Eqs. (5)–(8)], and is converted into the detector output voltage  $V$  as discussed above.

### III. TWO QUBITS MEASURED CONTINUOUSLY BY THE NON-LINEAR DETECTOR

The main focus of this work is on the measurement of the system of two, in general interacting, qubits. The qubit Hamiltonian is:

$$H_0 = -\frac{1}{2} \sum_{j=1,2} (\varepsilon_j \sigma_z^j + \Delta_j \sigma_x^j) + \frac{\nu}{2} \sigma_z^1 \sigma_z^2, \quad (12)$$

where  $\Delta_j$  is the tunnel amplitude and  $\varepsilon_j$  is the bias of the  $j$ -th qubit ( $j = 1, 2$ ),  $\nu$  is the qubit-qubit interaction energy, and  $\sigma$ 's here and below denote the Pauli matrices. The qubits are coupled to one detector (see Fig. 1) through their basis-forming variables  $\sigma_z^j$ , and the control operator  $x$  modulating the detector tunneling (1) is

$x = c_1 \sigma_z^1 + c_2 \sigma_z^2$ . It gives the following expression for the tunneling amplitude  $t$ :

$$\hat{t}(x) = t_0 + \sum_j \delta_j \sigma_z^j + \lambda \sigma_z^1 \sigma_z^2. \quad (13)$$

The last term in this expression appears due to non-linearity of the dependence of the transmission amplitude  $t$  on variable  $x$ . If the linear terms in Eq. (13) vanish,  $\delta_j = 0$ , while  $\lambda \neq 0$ , one has purely quadratic detector. In the case of two qubits, since the Pauli matrices satisfy the condition  $\sigma^2 = 1$ , Eq. (13) represents the most general dependence of  $t$  on  $\sigma_z^j$ .<sup>34</sup> In the example of the SQUID detector discussed in Sec. II, when the two flux qubits are coupled to it, the normalized flux  $\phi$  through the detector is:

$$\phi = \bar{\phi} + 2 \sum_j \delta \phi_j \sigma_z^j,$$

where  $\delta \phi_j$  characterizes the strength of coupling to the  $j$ th qubit, and the average flux  $\bar{\phi}$  sets the detector operating point. With such a coupling, the amplitude (9) of the Cooper-pair tunneling in the detector is given by Eq. (13) with

$$\begin{aligned} t_0 &= [i_1 e^{i\bar{\phi}/2} + i_2 e^{-i\bar{\phi}/2}] \cos \delta \phi_1 \cos \delta \phi_2, \\ \delta_j &= i[i_1 e^{i\bar{\phi}/2} - i_2 e^{-i\bar{\phi}/2}] \cos \delta \phi_{j'} \sin \delta \phi_j, \quad j' \neq j, \\ \lambda &= -[i_1 e^{i\bar{\phi}/2} + i_2 e^{-i\bar{\phi}/2}] \sin \delta \phi_1 \sin \delta \phi_2. \end{aligned}$$

If  $\bar{\phi} = 2\pi n$  with integer  $n$ , and the SQUID is symmetric:  $i_1 = i_2 = 1$ , the linear coupling coefficients  $\delta_j$  vanish and the SQUID has only quadratic response.

For qubit-detector coupling of the form (13), it is convenient to write the general equation (4) for the density matrix  $\rho$  of the two-qubit system in the “measurement” basis of eigenstates of the  $\sigma_z^j$  operators,  $|\uparrow\uparrow\rangle, |\uparrow\downarrow\rangle, |\downarrow\uparrow\rangle$ , and  $|\downarrow\downarrow\rangle$ . Each state  $|k\rangle$  of this basis is characterized by the magnitude  $t_k$  of the transmission amplitude (13):

$$\begin{aligned} t_1 &= t_0 + \delta_1 + \delta_2 + \lambda, & t_2 &= t_0 + \delta_1 - \delta_2 - \lambda, \\ t_3 &= t_0 - \delta_1 + \delta_2 - \lambda, & t_4 &= t_0 - \delta_1 - \delta_2 + \lambda, \end{aligned}$$

and associated value of the detector tunneling current, for which we use the obvious notations:

$$\begin{aligned} I_{\uparrow\uparrow} &= (\Gamma_+ - \Gamma_-) |t_0 + \delta_1 + \delta_2 + \lambda|^2, \\ I_{\uparrow\downarrow} &= (\Gamma_+ - \Gamma_-) |t_0 + \delta_1 - \delta_2 - \lambda|^2, \\ I_{\downarrow\uparrow} &= (\Gamma_+ - \Gamma_-) |t_0 - \delta_1 + \delta_2 - \lambda|^2, \\ I_{\downarrow\downarrow} &= (\Gamma_+ - \Gamma_-) |t_0 - \delta_1 - \delta_2 + \lambda|^2. \end{aligned}$$

Combining measurement-induced evolution (4) with the evolution due to the qubit Hamiltonian  $H_0$  we get the equation for  $\rho$  in the measurement basis:

$$\begin{aligned} \dot{\rho}_{kl} &= -\gamma_{kl} \rho_{kl} - i[H_0, \rho]_{kl}, \\ \gamma_{kl} &= (1/2)(\Gamma_+ + \Gamma_-) |t_k - t_l|^2. \end{aligned} \quad (14)$$

In Eq. (14), the Hamiltonian  $H_0$  includes two renormalization terms:

$$H_0 \rightarrow H_0 + \delta H + \delta H'.$$

The first one is due to imaginary parts of the correlators (2):

$$\delta H = \sum_j \delta \varepsilon_j \sigma_z^j + \delta \nu \sigma_z^1 \sigma_z^2 \quad (15)$$

where

$$\begin{aligned} \delta \varepsilon_j &= \text{Re}(\delta_j t_0^* + \delta_{j'} \lambda^*) \text{Im}(\gamma_- + \gamma_+), \\ \delta \nu &= \text{Re}(\delta_1 \delta_2^* + t_0 \lambda^*) \text{Im}(\gamma_- + \gamma_+), \end{aligned}$$

and  $j, j' = 1, 2$ , with  $j' \neq j$ . The second term  $\delta H'$  is due to phases  $\varphi_{kl} \equiv \arg(t_k t_l^*)$  of the transfer amplitudes  $t_k$  and is defined by the following relation:

$$[\delta H', \rho]_{kl} = (\Gamma_+ - \Gamma_-) |t_k t_l| \sin \varphi_{kl} \rho_{kl}. \quad (16)$$

Note that  $\delta H'$  can not always be cast in the form (15) in which it can be absorbed in the renormalization of qubit energies in the Hamiltonian (12). This can be done if the difference between the tunneling amplitudes  $t_k$  are small,  $|t_k - t_l| \ll |t_k|$ . In this work, we will assume that this condition on  $\delta H'$  is satisfied, and the renormalized Hamiltonian has the same form (12).

Equation (14) describes the time evolution of the qubits averaged over different measurement outcomes, which in our measurement model are represented by the number  $n$  of particles tunneled through the detector. Because of this averaging, the qualitative effect of measurement in Eq. (14) is the “back-action” dephasing of different states of the measurement basis with the rates  $\gamma_{kl}$ . In general, Eq. (4) contains information about the dynamics of  $n$  and can be used to write down the evolution equations conditioned on the specific measurement outcomes (see Ref. 9). The averaged equation (14) is sufficient for calculation of the output spectrum of the detector which is the purpose of this work.

The assumption of short detector tunneling time that lead to Eq. (14) makes this equation valid even in the regime when the detector-qubit coupling is strong and the dephasing rates  $\gamma_{kl}$  are large in comparison with the rates of evolution due to the Hamiltonian  $H_0$ . Straightforward numerical solution of Eq. (14) combined with Eqs. (7) and (8) gives the spectrum of the detector output. (All numerical plots of the spectra are obtained below in this way.) An example of such a spectrum for most generic set of parameters of the qubit-detector system is shown in Fig. 3. For these parameters all six intervals between four energy levels of the two-qubit Hamiltonian (12) are different, and show up as six finite-frequency peaks in the spectrum of the detector output. There is also the zero-frequency peak that reflects the dynamics of detector-induced transitions between the energy levels. Qualitatively, the width of all peaks corresponds to

the rates of transitions between the energy levels, with finite frequency peaks are also broadened by the “pure dephasing” terms in the evolution equation for the density matrix of the system [see Eq. (19) below] that are not related to the transitions.

Although so far the nonlinear mesoscopic detectors of the type considered in this work have not been realized experimentally, many elements of our detector model were indeed demonstrated. For instance, the QPC detector, which is the simplest realization of this model, was used to measure coherent oscillations in a quantum-dot qubit<sup>18</sup>. Parameters of the detector-qubit system used in Fig. 3 and other numerical results presented below (in particular the characteristic detector tunneling rate  $\Gamma_+ |t_0|^2$  on the order of the qubit oscillation frequency  $\Delta$ ) are consistent with those in experiments.

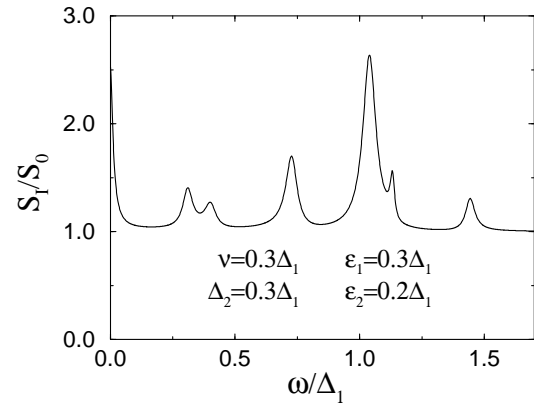


FIG. 3. Output spectrum of a nonlinear detector measuring two qubits with “the most general” set of parameters. Six peaks in the spectrum at finite frequencies correspond to six different energy intervals in the energy spectrum of the two-qubit system. The zero-frequency peak reflects dynamics of transitions between energy levels. Detector parameters are:  $\delta_1 = 0.1$ ,  $\delta_2 = 0.07$ ,  $\lambda = 0.09$  (all normalized to  $t_0$ ). In this Figure, and in all numerical plots below we take  $\Gamma_+ |t_0|^2 = \Delta_1$ ,  $\Gamma_- = 0$ , and assume that the detector tunneling amplitudes are real.

In the situation without any symmetries in the qubit parameters, matrix elements of the detector-qubit coupling are non-vanishing between all four energy eigenstates of the two-qubit system (12). Moreover, the assumption of the short detector tunneling time implies that the transition rate is independent of the energies of these states: i.e., if one views the detector as the reservoir producing dephasing for the measured system, the effective reservoir temperature is much larger than the system energies. This means that the stationary density matrix of the system is:

$$\rho_0 = \hat{I}/4, \quad (17)$$

where  $\hat{I}$  is the unity matrix in the four-dimensional space of the two-qubit system. This means that the dc detector current (6) in this regime is:

$$\begin{aligned}\langle I \rangle &= (I_{\uparrow\uparrow} + I_{\uparrow\downarrow} + I_{\downarrow\uparrow} + I_{\downarrow\downarrow})/4 \\ &= (\Gamma_+ - \Gamma_-)(|t_0|^2 + |\delta_1|^2 + |\delta_2|^2 + |\lambda|^2),\end{aligned}\quad (18)$$

and associated noise  $S_0$  (8) is given by the same expression with  $\Gamma_+ - \Gamma_-$  replaced by  $\Gamma_+ + \Gamma_-$ . If, however, the qubit parameters have some symmetry (examples are given in the Sections that follow), matrix elements satisfy “selection rules” and vanish for transitions into some states. The stationary density matrix  $\rho_0$  is then proportional to the unity matrix confined to a smaller subspace of the Hilbert space of the two-qubit system. In this case the dc current  $\langle I \rangle$  and the noise  $S_0$  are given by equations different from Eq. (18), and the number of peaks in the detector spectrum is less than the maximum of 6 peaks.

It is interesting to note that the selection rules that determine the number of finite-frequency peaks in the output spectrum of the detector allow sometimes for a simple qualitative classical interpretation. For instance, as will be demonstrated more rigorously below, in agreement with the case of classical oscillations, if the qubit-qubit interaction vanishes, and the detector is purely linear, the output spectrum contains at most two peaks that correspond to oscillations in the individual qubits with frequencies  $\Omega_{1,2}$ . If the detector is non-linear, the spectrum acquires two more peaks at the combination frequencies  $\Omega_1 \pm \Omega_2$ . The maximum total number of peaks is also equal to four if the detector is linear but the qubit-qubit interaction is finite.

Quantitatively, the detector spectrum can be obtained from the solution of Eq. (14) for evolution of the qubit density matrix. Despite the relative simplicity of its numerical solution, Eq. (14) can be solved analytically only in a few cases [see, e.g., Eq. (24) below]. More detailed analytical results can be obtained if the dephasing rates  $\gamma_{kl}$  are small in comparison to the intervals  $\omega_{nm} \equiv E_n - E_m$  between eigenenergies of the Hamiltonian  $H_0$  (12). In this limit, it is convenient to transform Eq. (14) into the basis of eigenstates  $|n\rangle$  of  $H_0$ ,  $H_0|n\rangle = E_n|n\rangle$ , where one can separate components of the density matrix  $\rho$  that evolve with different frequencies. Then, making use of the standard approach (see, e.g.,<sup>35</sup>) equation for  $\rho$  can be simplified by neglecting the terms that mix these components. Written in the energy eigenstate basis, Eq. (14) is reduced in this way to the following form:

$$\begin{aligned}\dot{\rho}_{nm} &= -i\omega_{nm}\rho_{nm} + (\Gamma_+ + \Gamma_-) \times \\ &\left[ - \left( \sum_{p \neq m} |\hat{t}_{mp}|^2 + \sum_{p \neq n} |\hat{t}_{np}|^2 + |\hat{t}_{mm} - \hat{t}_{nn}|^2 \right) \rho_{nm}/2 + \right. \\ &\left. \delta_{nm} \sum_p \rho_{pp} |\hat{t}_{mp}|^2 + (1 - \delta_{nm}) \sum_{(p,q)} \rho_{pq} \text{Re}(\hat{t}_{np}^* \hat{t}_{qm}) \right].\end{aligned}\quad (19)$$

where  $\hat{t}_{pq}$  are the matrix elements of the tunneling amplitude  $\hat{t}$  (as operator in the qubit space) in the basis of energy eigenstates, and the last sum is taken over the pairs  $(p, q)$  of states that satisfy the “resonance” condition:  $E_p - E_q = E_n - E_m$ ,  $(p, q) \neq (n, m)$ , and there-

fore contribute to the same spectral peak of the detector output. Solution of Eq. (19) can be used to calculate the average detector current and its spectrum using the same Eqs. (5)–(8). In the next Section, we use both Eq. (14) and Eq. (19) to describe the time evolution of the two-qubit system and resulting detector output in different situations.

#### IV. SPECTRAL DENSITY OF THE DETECTOR OUTPUT

Dynamics of the detector-qubit system and spectral density of the detector output depend on several characteristics of the system, most important of which are: the degree of non-linearity of the detector-qubit coupling, symmetry of parameters of individual qubits, and strength of the qubit-qubit interaction. In this Section, we calculate the spectra of the detector output in several regimes that differ in terms of these characteristics. Subsection A discusses the case of purely quadratic coupling of the detector to qubits that, in general, are different and interacting. Subsection B deals with the detector-qubit coupling which includes both the linear and quadratic terms but only for identical qubits. In the last Subsection C, we consider the most general case of different and interacting qubits measured by the detector with arbitrary non-linearity limiting ourselves to the regime of weak detector-qubit coupling.

##### A. Purely quadratic detector

We begin the discussion of the detector output spectrum by considering the purely quadratic measurement of *unbiased* qubits ( $\delta_j = \varepsilon_j = 0$ ). In this case, dynamics of measurement governed by Eq. (14) is such that the Hilbert space of the two-qubit system is split into two two-dimensional subspaces  $D_{\pm}$  with no transitions between them, so that the system evolves independently in each subspace. If the basis of states in the subspace  $D_{\pm}$  is chosen as

$$D_{\pm} \equiv \left\{ \frac{1}{\sqrt{2}}(|\uparrow\uparrow\rangle \pm |\downarrow\downarrow\rangle), \frac{1}{\sqrt{2}}(|\downarrow\uparrow\rangle \pm |\uparrow\downarrow\rangle) \right\}, \quad (20)$$

the Hamiltonian (12) is split into two independent parts  $H_{\pm}$  acting within  $D_{\pm}$ :

$$H_{\pm} = -(1/2)[(\Delta_1 \pm \Delta_2)\bar{\sigma}_x + \nu\bar{\sigma}_z]. \quad (21)$$

(By putting the bars on the Pauli matrices  $\sigma$  in this equation, we want to distinguish these Pauli matrices acting in the subspaces  $D_{\pm}$  from those describing individual qubits.)

Qualitatively, the qubit dynamics within each subspace can be viewed as oscillations between parallel and antiparallel configurations. The oscillation frequencies are

equal to  $\Delta_1 \pm \Delta_2$  for non-interacting qubits and are shifted upwards by interaction which creates energy difference between the parallel and anti-parallel configurations. Since the purely quadratic detector distinguishes these two types of qubit configurations, the current operator (5) within each subspace in the basis (20) is:

$$I = \langle I \rangle + I_a \bar{\sigma}_z, \quad (22)$$

where the average detector current  $\langle I \rangle$  is given by Eq. (18) with  $\delta_j = 0$ , and

$$I_a = (\Gamma_+ - \Gamma_-) 2\text{Re}(t_0 \lambda^*) = I_{\uparrow\uparrow} - I_{\uparrow\downarrow}$$

has the meaning of the amplitude of the detector current oscillations reflecting the qubit oscillations between the parallel and anti-parallel configurations.

Quantitatively, the evolution equation (14) within  $D_{\pm}$  is:

$$\dot{\rho}_{kl}^{(\pm)} = -i[H_{\pm}, \rho^{(\pm)}]_{kl} - \Gamma \begin{pmatrix} 0, & \rho_{12}^{(\pm)} \\ \rho_{21}^{(\pm)}, & 0 \end{pmatrix}, \quad (23)$$

where  $\Gamma \equiv 2(\Gamma_+ + \Gamma_-)|\lambda|^2$  is the measurement-induced dephasing of the basis states (20) of each subspace. For *non-interacting* qubits, solving this equation and calculating the spectral density of the detector output according to Eq. (7) we get<sup>9</sup>:

$$S_I^{\pm}(\omega) = S_0 + \frac{2I_a^2(\Delta_1 \pm \Delta_2)^2 \Gamma}{(\omega^2 - (\Delta_1 \pm \Delta_2)^2)^2 + \Gamma^2 \omega^2}, \quad (24)$$

where  $S_0 = (\Gamma_+ + \Gamma_-)(|t_0|^2 + |\lambda|^2)$ .

The two spectral densities (24) correspond to two possible outcomes of measurement: the qubits found in one or the other subspace  $D_{\pm}$ , the probability of the outcomes being determined by the initial state of the qubits. Each of the spectral densities coincides with the spectral density of the linear detector measuring coherent oscillations in one qubit<sup>2</sup>. Similarly to that case, the maximum of the ratio of the oscillation peak versus noise  $S_0$  for each spectrum  $S_I^{\pm}(\omega)$  is 4. As one can see from Eq. (24), this maximum is reached when the measurement is weak:  $|\lambda| \ll |t_0|$ , and the detector is “ideal”:  $\arg(t_0 \lambda^*) = 0$ , and only  $\Gamma_+$  or  $\Gamma_-$  is non-vanishing. If, however, there is small but finite transition rate between the two subspaces that mixes the two outcomes of measurement, the peak height is reduced by averaging over the two spectral densities (24). This situation is illustrated in Fig. 4 which shows the output spectra of the purely quadratic detector, when the subspaces  $D_{\pm}$  are mixed by small qubit bias  $\varepsilon$ . Since the stationary density matrix (17) is equally distributed over all qubit states, the two peaks of the spectral densities (24) are mixed with equal probabilities, and the maximum of the ratio of the oscillation peak heights versus noise  $S_0$  for the combined spectrum  $S_I(\omega)$  is 2. Spectrum shown in Fig. 4 for  $\varepsilon = 0.1\Delta_1$  (solid line) is close to this limit.

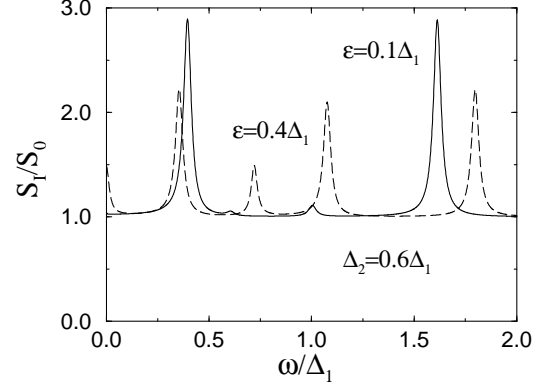


FIG. 4. Output spectra of a purely quadratic detector measuring two non-interacting qubits. Small qubit bias  $\varepsilon_1 = \varepsilon_2 \equiv \varepsilon$  (solid line) creates transitions that lead to averaging of the two main peaks at combination frequencies  $\Delta_1 \pm \Delta_2$  [see Eq. (24)]. Further increase of  $\varepsilon$  (dashed line) makes additional spectral peaks associated with these transitions more pronounced. The strength of quadratic qubit-detector coupling is taken to be  $\lambda = 0.15t_0$ .

For *interacting* qubits, analytical results for the spectrum can be obtained in the case of weak back-action dephasing  $\Gamma \ll |\Delta_1 \pm \Delta_2|$ , when the evolution equations (23) within each subspace can be transformed into the energy eigenstates representation and simplified there similarly to Eq. (19). In this limit, the shape of all spectral peaks is Lorentzian, with the decay rate  $\gamma$  of the off-diagonal elements of the density matrices  $\rho^{(\pm)}$  in the eigenstate representation,

$$\gamma = (\Gamma_+ + \Gamma_-)|\lambda|^2(1 + \nu^2/\Omega_{\pm}^2),$$

determines the width of the peaks at the combination frequencies shifted by interaction:

$$\Omega_{\pm} = [(\Delta_1 \pm \Delta_2)^2 + \nu^2]^{1/2}. \quad (25)$$

In the case of non-vanishing interaction strength  $\nu$ , the eigenstates of the Hamiltonians (21) have different amplitudes of states (20) with parallel and anti-parallel qubit configurations and therefore have different values of the average detector current (22). This means that for  $\Gamma \ll |\Delta_1 \pm \Delta_2|$ , nonvanishing interaction  $\nu$  creates the spectral peak at zero frequency which reflects the transitions between the energy eigenstates. The width of this peak  $\gamma_0$  is determined by the rate of transitions between these states:

$$\gamma_0 = 2(\Gamma_+ + \Gamma_-)|\lambda|^2(\Delta_1 \pm \Delta_2)^2/\Omega_{\pm}^2.$$

The total spectra  $S_I^{\pm}(\omega)$  within each subspace  $D_{\pm}$  are:

$$S_I^{\pm}(\omega) = S_0 + \frac{I_a^2}{\Omega_{\pm}^2} \left( \frac{2\nu^2\gamma_0}{\omega^2 + \gamma_0^2} + \left[ \frac{(\Delta_1 \pm \Delta_2)^2\gamma}{(\omega - \Omega_{\pm})^2 + \gamma^2} + (\omega \rightarrow -\omega) \right] \right). \quad (26)$$

Finite qubit bias should lead to averaging of the two spectra  $S_I^\pm$  (26) similar to that discussed in the case of non-interacting qubits and illustrated in Fig. 4.

If the difference of the qubit tunneling amplitudes become small,  $|\Delta_1 - \Delta_2| \ll \Gamma$ , qubit dynamics in the  $D_-$  subspace can no longer be viewed as coherent oscillations between the basis states (20), but rather as incoherent transitions between these states. The rate of these incoherent transition  $\tau^{-1}$  can be found by treating  $\Delta_1 - \Delta_2$  as perturbation in the evolution equation (23) for the density matrix  $\rho^{(-)}$ :

$$\tau^{-1} = \frac{1}{2} \frac{(\Delta_1 - \Delta_2)^2 \Gamma}{\nu^2 + \Gamma^2}. \quad (27)$$

Since the basis states (20) are characterized by different values  $\langle I \rangle + I_a$  of the detector current – see Eq. (22), these transition give rise to the spectral peak in the detector output spectrum at zero-frequency:

$$S_I^-(\omega) = S_0 + \frac{2I_a^2 \tau}{1 + \tau^2 \omega^2}, \quad \omega \simeq \tau^{-1}. \quad (28)$$

Equation (28) for the zero-frequency peak in the detector output is valid for arbitrary relation between the back-action dephasing rate and interaction strength  $\nu$ . It reproduces both the zero-frequency peak in the spectrum (26) when  $\Gamma \ll \nu$ , and if  $\Gamma \gg \nu$ , the peak in  $S_I^-$  obtained from Eq. (24) in the limit  $|\Delta_1 - \Delta_2| \ll \Gamma$ . If the qubits are identical,  $\Delta_1 = \Delta_2$ , the transitions (27) are suppressed and both basis states of the subspace  $D_-$  represent separate outcomes of quadratic measurement.

### B. Non-linear detector measuring identical qubits

In the case when the two qubits have the same set of parameters, it is convenient to discuss dynamics of the two-qubit system using the language of the total “spin”  $S = (\sigma_1 + \sigma_2)/2$ . The qubit Hamiltonian (12) and the detector tunnel amplitude (13) providing the qubit-detector coupling can be written in terms of  $S$  like this:

$$H_0 = -\varepsilon S_z - \Delta S_x + \nu S_z^2, \quad (29)$$

$$t = t_0 + 2\delta S_z + \lambda(2S_z^2 - 1), \quad (30)$$

where  $\varepsilon, \Delta, \delta$  without indices denote the same quantities as for individual qubits. The state  $(|\downarrow\uparrow\rangle - |\uparrow\downarrow\rangle)/\sqrt{2}$  with  $S = 0$  does not evolve in time under the Hamiltonian (29) and represents one of the measurement outcomes characterized by the dc detector current

$$\langle I \rangle = (\Gamma_+ - \Gamma_-)|t_0 - \lambda|^2$$

and flat output spectrum  $S_I(\omega) = (\Gamma_+ + \Gamma_-)|t_0 - \lambda|^2$ .

Three other,  $S = 1$ , states are mixed by measurement and represent the second measurement outcome. Inserting Eq. (30) into Eq. (5) and using the fact that in the

$S = 1$  subspace  $S_z^3 = S_z$ , we get the following expression for the detector current operator in this subspace:

$$I = (\Gamma_+ - \Gamma_-)|t_0 - \lambda|^2 + a_1 S_z + 2a_2 S_z^2, \quad (31)$$

where  $a_{1,2}$  have the meaning of the amplitudes of current oscillations between different qubit states:

$$a_1 = 4(\Gamma_+ - \Gamma_-)\text{Re}[(t_0 + \lambda)\delta^*] = (I_{\uparrow\uparrow} - I_{\downarrow\downarrow})/2, \quad (32)$$

$$a_2 = 2(\Gamma_+ - \Gamma_-)(\text{Re}[t_0\lambda^*] + |\delta|^2) = (I_{\uparrow\uparrow} + I_{\downarrow\downarrow} - 2I_{\uparrow\downarrow})/4.$$

Similarly to Eq. (17), the stationary density matrix within the  $S = 1$  subspace is  $\rho_0 = 1/3$ . Taking the average over the three eigenvalues of  $S_z$  operator,  $S_z = 0, \pm 1$ , with this density matrix, we see that the dc detector current in the measurement outcome that corresponds to the  $S = 1$  subspace is

$$\langle I \rangle = \frac{\Gamma_+ - \Gamma_-}{3} [2(|t_0|^2 + |\lambda|^2) + |t_0 + \lambda|^2 + 8|\delta|^2], \quad (33)$$

and can be written as  $\langle I \rangle = (I_{\uparrow\uparrow} + I_{\downarrow\downarrow} + I_{\uparrow\downarrow})/3$ .

To calculate the spectral density of the detector current (31), we consider first *non-interacting* qubits and limit ourselves to the case of weak measurement which can be described conveniently by going to the basis of the energy eigenstates. Using the vector intuition for spin operators, one sees directly that an appropriate rotation of the Hamiltonian (29) brings it to the form

$$H = -\Omega S_z, \quad \Omega = (\Delta^2 + \varepsilon^2)^{1/2}, \quad (34)$$

with three energies  $\{-\Omega, 0, \Omega\}$ . Upon this rotation, the operator  $S_z$  in the tunneling amplitude (30) changes accordingly

$$S_z \rightarrow (\varepsilon S_z + \Delta S_x)/\Omega. \quad (35)$$

In the regime of weak measurements, spectral peaks of the detector output at different frequencies are determined by the evolution of different groups of matrix elements of the operator  $s \equiv \rho_0 I$ , which evolve independently one from another. A peak at some finite frequency  $\bar{\omega}$  is determined by the off-diagonal matrix elements of  $s$  between the states with the energy difference equal to  $\bar{\omega}$ . This means that the total number of the matrix elements relevant for a given  $\bar{\omega}$  coincides with the number of times this interval occurs in the energy spectrum. In the situation considered in this subsection,  $s = I/3$ , where the current operator  $I$  is given by Eq. (31) in which  $S_z$  is transformed according to Eq. (35). The structure of the energy levels of the Hamiltonian (34) implies that there should be three peaks in the spectrum of the detector output: at  $\omega \simeq \Omega, 2\Omega$ , and the zero-frequency “relaxation” peak.

If the basis states are numbered in the direction of increasing energy,  $H|1\rangle = -\Omega|1\rangle$ ,  $H|2\rangle = 0$ , etc., the peak at  $\omega \simeq 2\Omega$  is determined by the matrix element  $s_{13}$  which satisfy the simple equation that follows from Eq. (19):

$$\dot{s}_{13} = (i2\Omega - \gamma)s_{13}, \quad (36)$$

and the initial condition  $s_{13}(0) = I_{13}/3$ , where

$$I_{13} = a_2 \Delta^2 / \Omega^2$$

is the matrix element of the current operator given by Eqs. (31) and (35). The decoherence rate  $\gamma$  in Eq. (36) is:

$$\gamma = \frac{1}{2} [\Gamma_{12} + \Gamma_{23} + 2\Gamma_{13} + (\Gamma_+ + \Gamma_-)(4\varepsilon|\delta|/\Omega)^2],$$

where the last term represents the pure dephasing, and  $\Gamma_{ij}$  is the rate of transitions between the states  $i$  and  $j$ :

$$\begin{aligned} \Gamma_{12} &= 2(\Gamma_+ + \Gamma_-)|\delta\Omega + \lambda\varepsilon|^2 \Delta^2 / \Omega^4, \\ \Gamma_{13} &= (\Gamma_+ + \Gamma_-)|\lambda|^2 \Delta^4 / \Omega^4, \end{aligned} \quad (37)$$

and the rate  $\Gamma_{23}$  is given by the same expression as  $\Gamma_{12}$  with  $\varepsilon \rightarrow -\varepsilon$ . All the rates are obtained from Eq. (19) in which the matrix elements of the operator of the tunnel amplitude are given by Eqs. (30) and (35). Equation (36) means that the spectral peak at  $\omega \simeq 2\Omega$  has simple Lorentzian form:

$$S_I(\omega) = S_0 + \frac{2}{3} \frac{(I_{13})^2 \gamma}{(\omega - 2\Omega)^2 + \gamma^2}, \quad (38)$$

and the background noise  $S_0$  coincides with Eq. (33) for the dc current in which  $\Gamma_+ - \Gamma_-$  is replaced by  $\Gamma_+ + \Gamma_-$ .

The structure of the  $\omega \simeq \Omega$  peak of the spectral density of the detector output is determined by the time evolution of the matrix elements  $s_{12}$  and  $s_{23}$  which satisfy the coupled system of equations following from Eq. (19):

$$\begin{aligned} \dot{s}_{12} &= i\Omega s_{12} - \xi_1 s_{12} + \kappa s_{23}, \\ \dot{s}_{23} &= i\Omega s_{23} - \xi_2 s_{23} + \kappa s_{12}. \end{aligned} \quad (39)$$

Initial conditions in these equations are the same as in Eq. (36),  $s_{ij}(0) = I_{ij}/3$ , where the current matrix elements are:

$$I_{12} = a_1(\Delta/\sqrt{2}\Omega) + a_2(\sqrt{2}\varepsilon\Delta/\Omega^2),$$

and  $I_{23}$  is given by the same expression with  $\varepsilon \rightarrow -\varepsilon$ . Again, the relaxation rates  $\xi_m$ ,  $m = 1, 2$ , and the rate  $\kappa$  of the “transfer of coherence” are obtained by combining the matrix elements of the transmission amplitude (30), (35) with Eq. (19):

$$\begin{aligned} \xi_m &= (\Gamma_+ + \Gamma_-)[|\delta|^2(2 + \Delta^2/\Omega^2) - (-1)^m \\ &\quad \times 4\text{Re}(\delta\lambda^*)(\varepsilon/\Omega)^3 + |\lambda|^2(\Delta^4 + \varepsilon^2\Delta^2 + 2\varepsilon^4)/\Omega^4], \\ \kappa &= (\Gamma_+ + \Gamma_-)(|\delta|^2\Omega^2 - |\lambda|^2\varepsilon^2)(2\Delta^2/\Omega^4). \end{aligned}$$

Solving Eq. (39) by diagonalization of the matrix of evolution coefficients, we see that the spectral peak at  $\omega \simeq \Omega$  consists in general of two overlapping Lorentzians with different line-widths and amplitudes:

$$S_I(\omega) = S_0 + \frac{1}{3} \sum_{m=1,2} \frac{A_m \gamma_m}{(\omega - \Omega)^2 + \gamma_m^2}, \quad (40)$$

where

$$\begin{aligned} \gamma_m &= (\xi_1 + \xi_2)/2 + (-1)^m D, \\ D &\equiv [(\xi_1 - \xi_2)^2/4 + \kappa^2]^{1/2}, \\ A_m &= I_1^2 + I_2^2 - \frac{(-1)^m}{D} [2I_1 I_2 \kappa - (I_1^2 - I_2^2) \frac{\xi_1 - \xi_2}{2}], \end{aligned} \quad (41)$$

where for later convenience we introduced notations:  $I_1 \equiv I_{12}$ ,  $I_2 \equiv I_{23}$ . In the case of unbiased qubits,  $\varepsilon = 0$ , the situation becomes much simpler:  $\xi_1 = \xi_2$ ,  $I_{12} = I_{23}$ , and one of the Lorentzians vanishes,  $A_2 = 0$ . In this case the peak at  $\omega \simeq \Omega$  has the form of one Lorentzian with the line-width  $\gamma_1 = (\Gamma_+ + \Gamma_-)(|\delta|^2 + |\lambda|^2)$  and amplitude  $A_1 = 2a_1^2$ . For purely linear measurement:  $\lambda = 0$ ,  $|\delta| \ll |t_0|$ , this implies that the maximum peak height  $2a_1^2/3\gamma_1$  is limited by  $(32/3)S_0$ .<sup>36</sup>

The spectral peak at  $\omega \simeq 0$  is determined by the transitions between the energy eigenstates with the rates (37). The average current  $I_{jj}$  in the  $j$ -th state is different from the dc current (33) through the detector:

$$\begin{aligned} I_{11} - \langle I \rangle &= a_1(\varepsilon/\Omega) + a_2(2\varepsilon^2 - \Delta^2)/3\Omega^2, \\ I_{22} - \langle I \rangle &= 2a_2(\Delta^2 - 2\varepsilon^2)/3\Omega^2, \\ I_{33} - \langle I \rangle &= -a_1(\varepsilon/\Omega) + a_2(2\varepsilon^2 - \Delta^2)/3\Omega^2, \end{aligned} \quad (42)$$

Because of nonvanishing differences  $I_{jj} - \langle I \rangle$ , transitions between the eigenstates generate low-frequency noise in the detector current. Quantitatively, solving the standard kinetic equation for the evolution of occupation probabilities of the three eigenstates due to transitions (37) and substituting the solution into Eq. (7) we see that similarly to the peak at  $\omega \simeq \Omega$ , the zero-frequency peak of the spectral density of the detector output consists of two overlapping Lorentzians with different widths  $\eta_m$  and amplitudes  $B_m$ :

$$S_I(\omega) = S_0 + \frac{1}{3} \sum_{m=1,2} \frac{B_m \eta_m}{\omega^2 + \eta_m^2}, \quad (43)$$

Parameters of the two Lorentzians are determined by the transition rates (37) and the currents (42):

$$\begin{aligned} \eta_m &= \Gamma_{12} + \Gamma_{23} + \Gamma_{13} - (-1)^m D, \\ D &= [\Gamma_{12}^2 + \Gamma_{23}^2 + \Gamma_{13}^2 - \Gamma_{12}\Gamma_{23} - \Gamma_{12}\Gamma_{13} - \Gamma_{13}\Gamma_{23}]^{1/2}, \\ B_m &= [c_m a_1^2(\varepsilon/\Omega)^2 + c_{m'} a_2^2(\Delta^2 - 2\varepsilon^2)^2/3\Omega^4 \\ &\quad + (-1)^m (\Gamma_{12} - \Gamma_{23}) 2a_1 a_2 \varepsilon (\Delta^2 - 2\varepsilon^2)/\Omega^3]/D, \\ c_m &= 2D + (-1)^m (\Gamma_{12} + \Gamma_{23} - 2\Gamma_{13}), \end{aligned}$$

where  $m'$  is defined as  $m' = 1, 2$ ,  $m' \neq m$ .

The situation again simplifies drastically for unbiased qubits,  $\varepsilon \rightarrow 0$ , when only one of the Lorentzians has non-vanishing amplitude  $B = 2a_2^2/3$ . The width of this non-vanishing Lorentzian is

$$\eta = 3(\Gamma_{12} + \Gamma_{23})/2 = 6(\Gamma_+ + \Gamma_-)|\delta|^2.$$

Equations (38), (40), and (43) describe completely the output spectrum of the detector weakly coupled to identical non-interacting qubits. In agreement with classical intuition, the spectral peak at twice the frequency  $\Omega$  of the oscillations in individual qubits appears only if the detector-qubit coupling is effectively non-linear, when either  $\lambda \neq 0$  or  $\delta$  is not too small. The peak at individual qubit frequency  $\Omega$  has generically larger amplitude than the peak at  $2\Omega$  and can be viewed as the result of coherent superposition of oscillations in two qubits. (Note that the maximum peak height,  $(32/3)S_0$ , at  $\omega \simeq \Omega$  is larger than two times the height,  $4S_0$ , of the spectral peak associated with the oscillations in individual qubits.) This interpretation is supported by the behavior of the two peaks as a function of weak *qubit-qubit interaction*  $\nu$  which we consider now. Including the interaction term in the Hamiltonian (29) in the evolution equation for the density matrix in the basis of energy eigenstates (34) one can see that the interaction has no effect on the dynamics at  $\omega \simeq 2\Omega$  until interaction strength  $\nu$  becomes comparable to  $\Omega$ .

In contrast to this, the dynamics at  $\omega \simeq \Omega$  is affected by much weaker interaction on the order of the detector-induced dephasing. The interaction breaks coherence between oscillations in the two qubits and eventually splits the spectral peak at  $\omega \simeq \Omega$  in two as the interaction strength  $\nu$  becomes larger than dephasing. We describe this splitting quantitatively limiting ourselves to the case of unbiased qubits, when  $\Omega = \Delta$ . In the regime of weak interaction  $\nu \ll \Delta$ , we can use the “rotating-wave” approximation by keeping only those interaction terms in the evolution equations that do not mix components oscillating with different large frequencies on the order of  $\Delta$ . In this case, the peak at  $\omega \simeq \Delta$  is governed by the dynamics of the same matrix elements  $s_{12}$ ,  $s_{23}$ , as for non-interacting qubits, and Eqs. (39) for the dynamics of these elements now are:

$$\begin{aligned} \dot{s}_{12} &= i(\Delta + \nu/2)s_{12} - \xi s_{12} + \kappa s_{23}, \\ \dot{s}_{23} &= i(\Delta - \nu/2)s_{23} - \xi s_{23} + \kappa s_{12}, \end{aligned} \quad (44)$$

where we took into account that for vanishing bias,

$$\xi_1 = \xi_2 = (\Gamma_+ + \Gamma_-)(3|\delta|^2 + |\lambda|^2) \equiv \xi.$$

We see that for  $\nu \ll \Delta$ , the effect of the interaction is just the shift of energy of the zero-energy eigenstate of the Hamiltonian (34) by  $\nu/2$  relative to the two other eigenstates.

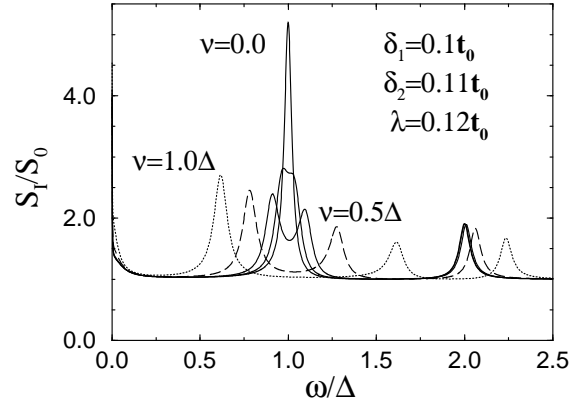


FIG. 5. Evolution of the output spectrum of the non-linear detector measuring two identical unbiased qubits with the strength  $\nu$  of the qubit-qubit interaction. The qubit-detector coupling constants  $\delta_{1,2}$  are taken to be slightly different to average the spectrum over all qubit states. The three solid curves correspond to  $\nu/\Delta = 0.0, 0.1, 0.2$ . In agreement with Eqs. (45) – (47), the peak at  $\omega \simeq \Delta$  is at first suppressed and then split in two by increasing  $\nu$ , while the peak at  $\omega \simeq 2\Delta$  is not changed noticeably by such a weak interaction. Dashed and dotted lines show the regime of relatively strong interaction:  $\nu/\Delta = 0.5$  and  $\nu/\Delta = 1.0$ , respectively, that is described by Eqs. (49) and (50).

Equations (44) have the same structure as Eqs. (39), and for weak interaction,  $\nu/2 < \kappa = 2(\Gamma_+ + \Gamma_-)|\delta|^2$ , result in the same form of the peak of the spectral density at  $\omega \simeq \Delta$  as in Eq. (40): two overlapping Lorentzians with different line-width  $\gamma_m$  and amplitudes  $A_m$ ,  $m = 1, 2$ :

$$\begin{aligned} \gamma_m &= \xi + (-1)^m D, \quad D = [\kappa^2 - \nu^2/4]^{1/2}, \\ A_m &= a_1^2(1 - (-1)^m \kappa/D). \end{aligned} \quad (45)$$

If  $\nu/2 \rightarrow \kappa$ , then  $D \rightarrow 0$ , and the two Lorentzians combine to give the peak of the following form:

$$S_I(\omega) = S_0 + \frac{2a_1^2}{3}(1 - \kappa \frac{\partial}{\partial \xi}) \frac{\xi}{(\omega - \Delta)^2 + \xi^2}. \quad (46)$$

For stronger interaction,  $\nu/2 > \kappa$ , the two Lorentzians acquire different frequencies  $\Delta \pm D$ ,  $D = [\nu^2/4 - \kappa^2]^{1/2}$ , while having the same line-width  $\xi$ , so that the total spectral density at  $\omega \simeq \Delta$  is:

$$S_I(\omega) = S_0 + \frac{a_1^2}{3} \sum_{\pm} \frac{\xi + \kappa \pm (\Delta - \omega)\kappa/D}{(\omega - \Delta \mp D)^2 + \xi^2}. \quad (47)$$

For  $\nu \gg \kappa$ , spectral density (47) consists of two independent Lorentzians separated by the large frequency interval  $\nu$ . The amplitude of both peaks is  $a_1^2/3\xi$  and is limited by  $(16/9)S_0$ , the value that should be reached by an ideal linear detector.

Equations (45), (46), and (47) are valid in the regime of weak interaction,  $\nu \simeq \kappa \ll \Delta$ , when interaction affects strongly only the spectral peak at  $\omega \simeq \Delta$ , which is first

broadened and then split in two with increasing interaction strength. To describe the detector output spectrum for stronger interaction  $\nu \simeq \Delta \gg \kappa$ , we need to diagonalize the Hamiltonian (29) with non-vanishing  $\nu$ . This can be done easily in the case of unbiased qubits  $\varepsilon = 0$ , when the eigenstates of the Hamiltonian (29) coincide with the two eigenstates of the Hamiltonian  $H_+$  (21) and the state  $(|\uparrow\uparrow\rangle - |\downarrow\downarrow\rangle)/\sqrt{2}$  of the subspace  $D_-$  introduced before in Eq. (20). The eigenenergies of these states are:

$$\{-\Omega_+/2, \nu/2, \Omega_+/2\}, \quad \Omega_+ = (4\Delta^2 + \nu^2)^{1/2}. \quad (48)$$

The three finite-frequency peaks in the spectrum correspond to three energy intervals,  $\Omega_+$ ,  $(\Omega_+ \pm \nu)/2$  in the spectrum of these eigenstates. Since all energy intervals are different and therefore there is no transfer of coherence between them that exists, e.g., in Eqs. (39), the peaks are simple Lorentzians. Transforming the tunneling amplitude (30) into the basis of eigenstates (48), we find all the rates in the evolution Eq. (19) and the matrix elements of the current operator (31) in this basis and find the parameters of these Lorentzians: amplitude  $A$  and the line-width  $\gamma$ , both defined as in Eq. (40):

$$\begin{aligned} \omega &\simeq \Omega_+, \quad A = 8(a_2\Delta/\Omega_+)^2, \\ \gamma &= (\Gamma_+ + \Gamma_-)[2|\delta|^2 + (1 + \nu^2/\Omega_+^2)|\lambda|^2], \end{aligned} \quad (49)$$

$$\begin{aligned} \omega &\simeq (\Omega_+ \pm \nu)/2, \quad A = a_1^2(1 \mp \nu/\Omega_+), \\ \gamma &= (\Gamma_+ + \Gamma_-)[3(1 \mp \nu/\Omega_+)|\delta|^2 + (1 \pm \nu/\Omega_+)|\lambda|^2]. \end{aligned} \quad (50)$$

One can see that parameters of the two lower-frequency peaks (50) agree in the regime  $\Delta \gg \nu \gg \kappa$  with the peaks in the spectral density (47), while the peak (49) at the largest frequency  $\Omega_+$  coincides with that described by Eq. (38) the case of unbiased non-interacting qubits.

Figure 5 illustrates evolution of the output spectrum of the non-linear detector measuring identical qubits due to changing interaction strength. We see that this evolution agrees with the analytical description developed above. Weak qubit-qubit interaction  $\nu \simeq \kappa \ll \Delta$  suppresses and subsequently splits the spectral peak at  $\omega \simeq \Omega$  while not changing the peak  $\omega \simeq 2\Omega$ . Stronger qubit-qubit interaction  $\nu \simeq \Delta \gg \kappa$  shifts the  $\omega \simeq 2\Omega$  peak to higher frequencies while moving the two peaks around  $\omega \simeq \Omega$  further apart.

### C. Non-linear detector measuring different qubits

As the last example of the output spectrum of the non-linear detector measuring two qubits we consider the most general situation when both the tunneling amplitudes and the detector-qubit coupling constants are different for the two qubits. We assume that the qubit parameters are such that all energy intervals in the spectrum of eigenstates are larger than the back-action dephasing rate, i.e., the detector-qubit coupling is weak. We begin with the case of *unbiased qubits*,  $\varepsilon_j = 0$ , when

the coherent oscillations in the two qubits should have the largest amplitude. At this bias point, the Hamiltonian (12) breaks into two subspaces  $D_\pm$  (20) and can be diagonalized directly. It is convenient to order the eigenstates taking into account these subspaces:

$$\{\Omega_+/2, -\Omega_+/2, \Omega_-/2, -\Omega_-/2\}. \quad (51)$$

The energies  $\Omega_\pm$  are defined in Eq. (25). The wavefunctions of the eigenstates numbered in this order are:

$$\begin{aligned} |\psi_1\rangle &= [(\alpha + \beta)(|\uparrow\uparrow\rangle + |\downarrow\downarrow\rangle) + (\beta - \alpha)(|\uparrow\downarrow\rangle + |\downarrow\uparrow\rangle)]/2, \\ |\psi_2\rangle &= [(\alpha - \beta)(|\uparrow\uparrow\rangle + |\downarrow\downarrow\rangle) + (\alpha + \beta)(|\uparrow\downarrow\rangle + |\downarrow\uparrow\rangle)]/2, \\ |\psi_3\rangle &= [(\bar{\alpha} + \bar{\beta})(|\uparrow\uparrow\rangle - |\downarrow\downarrow\rangle) + (\bar{\beta} - \bar{\alpha})(|\uparrow\downarrow\rangle - |\downarrow\uparrow\rangle)]/2, \\ |\psi_4\rangle &= [(\bar{\alpha} - \bar{\beta})(|\uparrow\uparrow\rangle - |\downarrow\downarrow\rangle) + (\bar{\alpha} + \bar{\beta})(|\uparrow\downarrow\rangle - |\downarrow\uparrow\rangle)]/2, \end{aligned}$$

where

$$\begin{aligned} \alpha, \beta &= (1/\sqrt{2})[1 \pm (\Delta_1 + \Delta_2)/\Omega_+]^{1/2}, \\ \bar{\alpha}, \bar{\beta} &= (1/\sqrt{2})[1 \pm (\Delta_1 - \Delta_2)/\Omega_-]^{1/2}. \end{aligned}$$

Assuming that there are no “accidental” degeneracies, there are four different energy intervals in the spectrum (51) which should be reflected as four finite-frequency peaks in the detector output spectrum. For different qubit parameters, there are no selection rules and the detector back-action mixes all four state of the qubit system. The stationary density matrix is then given by Eq. (17) and the background detector noise  $S_0$  corresponds to the dc current (18). The largest ( $\Omega_+$ ) and the smallest ( $\Omega_-$ ) energy intervals occur only once in the spectrum (51), so that the peaks at  $\omega \simeq \Omega_\pm$  has the shape of simple Lorentzians:

$$\omega \simeq \Omega_\pm, \quad S_I(\omega) = S_0 + \frac{1}{4} \frac{A_\pm \gamma_\pm}{(\omega - \Omega_\pm)^2 + \gamma_\pm^2}. \quad (52)$$

Calculating the current matrix elements and all the rates in Eq. (19) for evolution of the density matrix in the basis of eigenstates (51) similarly to what is done for the description of decoherence in coupled qubits<sup>37</sup>, we find parameters of the Lorentzians in Eq. (52). It is convenient to express the peak amplitudes  $A_\pm$  through the characteristic amplitudes of current modulation by the qubits analogous to the amplitudes  $a_{1,2}$  (32) for identical qubits. In the case of different strength of the detector-qubit coupling for the two qubits, we have three such amplitudes:

$$\begin{aligned} a_{11} &= (I_{\uparrow\uparrow} + I_{\uparrow\downarrow} - I_{\downarrow\uparrow} - I_{\downarrow\downarrow})/4 \\ &= 2(\Gamma_+ - \Gamma_-)\text{Re}[t_0\delta_1^* + \lambda\delta_2^*], \\ a_{12} &= (I_{\uparrow\uparrow} + I_{\downarrow\uparrow} - I_{\uparrow\downarrow} - I_{\downarrow\downarrow})/4 \\ &= 2(\Gamma_+ - \Gamma_-)\text{Re}[t_0\delta_2^* + \lambda\delta_1^*], \\ a_2 &= (I_{\uparrow\uparrow} + I_{\downarrow\downarrow} - I_{\uparrow\downarrow} - I_{\downarrow\uparrow})/4 \\ &= 2(\Gamma_+ - \Gamma_-)\text{Re}[t_0\lambda^* + \delta_1\delta_2^*]. \end{aligned} \quad (53)$$

For identical qubits,  $a_{11}$  and  $a_{12}$  reduce to  $a_1/2$ , while the definition of  $a_2$  in Eqs. (53) and (32) coincide. Qualitatively,  $a_{1j}$  corresponds to the amplitude of modulation of the detector current due to oscillations in the  $j$ -th

qubit, and  $a_2$  - is the similar amplitude due to “collective” oscillations of the two qubits between parallel and anti-parallel configurations. In terms of the amplitudes (53),  $A_{\pm}$  are given by simple expressions:

$$A_{\pm} = 2a_2^2[(\Delta_1 \pm \Delta_2)/\Omega_{\pm}]^2 \quad (54)$$

The line-widths  $\gamma_{\pm}$  in Eq. (52) are:

$$\gamma_{\pm} = (\Gamma_+ + \Gamma_-)[|\delta_1|^2 + |\delta_2|^2 + |\lambda|^2(1 + \nu^2/\Omega_{\pm}^2)]. \quad (55)$$

In contrast to the energy intervals  $\Omega_{\pm}$  which occur only once in the energy spectrum (51), the intervals  $(\Omega_+ \pm \Omega_-)/2$  occur twice each. This means that the spectral peaks at  $\omega \simeq (\Omega_+ \pm \Omega_-)/2$  are not simple Lorentzians, and their shape is controlled by the two matrix elements of the density matrix evolving according to a system of coupled equations identical with Eqs. (44). This means that these peaks consist of two overlapping Lorentzians each, and the output spectrum in their vicinity is given by the equation similar to Eq. (40):

$$S_I(\omega) = S_0 + \frac{1}{4} \sum_{m=1,2} \frac{A_m^{(\pm)} \gamma_m^{(\pm)}}{[\omega - (\Omega_+ \pm \Omega_-)/2]^2 + [\gamma_m^{(\pm)}]^2},$$

for  $\omega \simeq (\Omega_+ \pm \Omega_-)/2$ . Here the amplitudes  $A_m^{(\pm)}$  and line-widths  $\gamma_m^{(\pm)}$  are given by the same Eqs. (41), where now

$$\begin{aligned} \xi_m^{(\pm)} &= (\Gamma_+ + \Gamma_-) \left[ \left(1 \pm \frac{\nu^2}{\Omega_+ \Omega_-}\right) |\lambda|^2 + |\delta_1|^2 + |\delta_2|^2 \right. \\ &\quad \left. - (-1)^m \left(\frac{\nu}{\Omega_+} \mp \frac{\nu}{\Omega_-}\right) \text{Re}(\delta_1 \delta_2^*) \right] \\ \kappa^{(\pm)} &= \frac{1}{2} (\Gamma_+ + \Gamma_-) \left[ \frac{\Delta_1^2 - \Delta_2^2}{\Omega_+ \Omega_-} (|\delta_1|^2 + |\delta_2|^2) \right. \\ &\quad \left. - \left(\frac{\nu^2}{\Omega_+ \Omega_-} \pm 1\right) (|\delta_1|^2 - |\delta_2|^2) \right], \\ I_m^{(\pm)} &= (\pm 1)^{m+1} \frac{a_{11}}{\sqrt{2}} \left[ 1 \mp \frac{\nu^2 - \Delta_1^2 + \Delta_2^2}{\Omega_+ \Omega_-} \right]^{1/2} \\ &\quad + (\mp 1)^m \frac{a_{12}}{\sqrt{2}} \left[ 1 \mp \frac{\nu^2 + \Delta_1^2 - \Delta_2^2}{\Omega_+ \Omega_-} \right]^{1/2}. \end{aligned} \quad (56)$$

In the case of non-interacting qubits and no quadratic coupling,  $\nu = \lambda = 0$ , the peaks at  $(\Omega_+ \pm \Omega_-)/2$  represent oscillations in the individual qubits: the peak at  $(\Omega_+ - \Omega_-)/2$  describes oscillations in a qubit with a smaller  $\Delta$ , while the peak at  $(\Omega_+ + \Omega_-)/2$  - in the qubit with larger  $\Delta$ . Only one Lorentzian ( $m = 1$ ) is then non-vanishing for each peak, and has the same parameters as it would have in the absence of the other qubit. For instance, if  $\Delta_1 > \Delta_2$ , we get from Eqs. (41) and (56) for  $\nu = \lambda = 0$ :

$$\begin{aligned} (\Omega_+ + \Omega_-)/2 &= \Delta_1, \quad \gamma_1^{(+)} = (\Gamma_+ + \Gamma_-)|\delta_1|^2, \quad A_1^{(+)} = 4a_{11}^2, \\ (\Omega_+ - \Omega_-)/2 &= \Delta_2, \quad \gamma_1^{(-)} = (\Gamma_+ + \Gamma_-)|\delta_2|^2, \quad A_1^{(-)} = 4a_{12}^2. \end{aligned}$$

This behavior is the natural consequence of the linearity of the detector-qubit system for  $\nu = \lambda = 0$ .

Non-vanishing qubit-qubit interaction and/or non-linear detector response modify parameters of these “linear” peaks according to Eqs. (41) and (56). In contrast to these peaks, the spectral peaks at  $\Omega_{\pm}$  reflect directly the detector non-linearity and vanish in the linear regime when  $\lambda = 0$  and  $\delta_j \ll t_0$ . As one can see from Eq. (53), the characteristic amplitude  $a_2$  of these peaks scales for  $\lambda = 0$  as a higher power of  $\delta_j$  than the amplitudes  $a_{1j}$  of the linear peaks.

An example of the output spectrum of the non-linear detector measuring unbiased qubits with different tunneling amplitudes is shown in Fig. 6. One can see that when the linear and non-linear coefficient of the detector-qubit coupling are roughly similar, the linear peaks are more pronounced than the peaks at combination frequencies. Qubit-qubit interaction shifts all but the lower-frequency linear peak up in frequency and reduces both the amplitudes of the higher-frequency peaks and the distance between them.

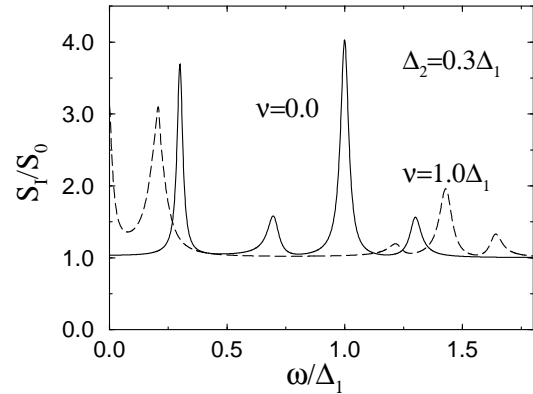


FIG. 6. Output spectra of the non-linear detector measuring two different unbiased qubits. Solid line is the spectrum in the case of non-interacting qubits. The two larger peaks are the “linear” peaks that correspond to the oscillations in the individual qubits, while smaller peaks are non-linear peaks at the combination frequencies. Dashed line is the spectrum for interacting qubits. Interaction shifts the lower-frequency linear peak down and all other peaks up in frequency. Parameters of the detector-qubit coupling are:  $\delta_1 = 0.12t_0$ ,  $\delta_2 = 0.09t_0$ ,  $\lambda = 0.08t_0$ .

Analytical results of this subsection can be easily extended to the finite qubit bias if the qubits are *non-interacting*. The eigenstates of the Hamiltonian (12) are then the products of the eigenstates of the individual qubits, so that the energy spectrum of the two-qubit system is:

$$(1/2)\{\Omega_1 + \Omega_2, \Omega_1 - \Omega_2, \Omega_2 - \Omega_1, -(\Omega_1 + \Omega_2)\}, \quad (57)$$

where  $\pm\Omega_j/2$  with  $\Omega_j = (\varepsilon_j^2 + \Delta_j^2)^{1/2}$  are the eigenenergies of the  $j$ -th qubit.

Similarly to the spectrum (51), there are four different energy intervals in (57). Two of them,  $\Omega_1 \pm \Omega_2 \equiv \Omega_{\pm}$  occur only once and are reflected as simple Lorentzian peaks in the detector output spectrum. These “non-linear”

peaks represent the mixture of the individual qubit oscillations with frequencies  $\Omega_{1,2}$  and have non-vanishing amplitude only if the detector response is non-linear. Quantitatively, the output spectrum around this peaks can be written as in Eq. (52), where now the peak parameters are:

$$A_{\pm} = 2a_2^2 \left( \frac{\Delta_1 \Delta_2}{\Omega_1 \Omega_2} \right)^2, \quad \gamma_{\pm} = (\Gamma_+ + \Gamma_-) [|\lambda|^2 \cdot [1 - \left( \frac{\varepsilon_1 \varepsilon_2}{\Omega_1 \Omega_2} \right)^2] + |\delta_1|^2 + |\delta_2|^2 + \left| \delta_1 \frac{\varepsilon_1}{\Omega_1} \pm \delta_2 \frac{\varepsilon_2}{\Omega_2} \right|^2]. \quad (58)$$

They are found by calculating both the rates in Eq. (19) for the density matrix, and the matrix elements of the current operator  $I$ :

$$I = \langle I \rangle + \sum_j a_{1j} \bar{\sigma}_z^j + a_2 \bar{\sigma}_z^1 \bar{\sigma}_z^2, \quad \bar{\sigma}_z^j = \frac{1}{\Omega_j} (\varepsilon_j \sigma_z^j + \Delta_j \sigma_x^j),$$

in the basis of states (57). In this expression,  $\langle I \rangle$  is the average current (18).

The energy intervals  $\Omega_j$  occur twice each in the spectrum (57). This means that the spectral peaks at  $\omega \simeq \Omega_j$  that correspond to the individual qubit oscillations have the same form as in Eq. (40), so that

$$S_I(\omega) = S_0 + \frac{1}{4} \sum_{m=1,2} \frac{A_{jm} \gamma_{jm}}{(\omega - \Omega_j)^2 + \gamma_{jm}^2} \quad (59)$$

for  $\omega \simeq \Omega_j$ , where the amplitudes  $A_{jm}$  and line-widths  $\gamma_{jm}$  are given by Eqs. (41) with

$$\begin{aligned} \xi_{jm} &= (\Gamma_+ + \Gamma_-) [(1 + [\varepsilon_j / \Omega_j]^2) |\delta_j - (-1)^m \lambda (\varepsilon_{j'} / \Omega_{j'})|^2 \\ &\quad + (|\lambda|^2 + |\delta_{j'}|^2) (\Delta_{j'} / \Omega_{j'})^2], \\ \kappa_j &= (\Gamma_+ + \Gamma_-) (\Delta_{j'} / \Omega_{j'})^2 [|\delta_{j'}|^2 + |\lambda|^2 (\varepsilon_j / \Omega_j)^2], \\ I_{jm} &= [a_{1j} - (-1)^m a_2 (\varepsilon_{j'} / \Omega_{j'})] (\Delta_j / \Omega_j), \end{aligned}$$

where  $j' \neq j$ .

We see from Eq. (59) that for non-interacting qubits, the non-vanishing qubit bias just shifts the frequency position of the linear peaks (56) without qualitatively changing their shape. If both the bias and the qubit-qubit interaction are finite, the bias splits each of the linear peaks in two simple Lorentzians bringing the total number of the finite-frequency peaks in the spectrum of the detector output to six as it should be in the generic situation (see, e.g., Fig. 3).

## V. CONCLUSION

To summarize, we have developed a theory of continuous quantum measurements of coherent oscillations in two coupled qubits by a non-linear detector. Calculated spectra of the detector output show that the detector non-linearity leads to the appearance of the spectral

peaks at the combination frequencies of the qubit oscillations in the detector output. The spectra have the non-trivial dependence on the strength of the qubit-qubit interaction. For identical non-interacting qubits, the spectral peaks at frequency of individual qubit oscillations are superimposed coherently, with weak interaction breaking this coherent superposition and splitting the oscillation peak. In general, qubit-qubit interaction should manifest itself qualitatively through the total number of peaks in the output spectrum: the total number of peaks is at most 4 in the case of non-interacting qubits, while it can reach 6 in the most general situation with both non-vanishing qubit-qubit interaction and the detector non-linearity.

## VI. ACKNOWLEDGMENTS

W.M. and D.V.A. would like to thank A.N. Korotkov and R. Ruskov for useful discussions at the initial stages of this work. This work was supported in part by the NSF under grant # 0121428 and by ARDA and DOD under the DURINT grant # F49620-01-1-0439 (W.M. and D.V.A.), and by the EC contracts IST-SQUBIT2 and RTN-Nanoscale Dynamics (F.P. and R.F.).

- 
- <sup>1</sup> "Quantum noise in mesoscopic physics" Ed. by Yu.V. Nazarov, (Kluwer, 2003).
  - <sup>2</sup> A.N. Korotkov and D.V. Averin, Phys. Rev. B **64**, 165310 (2001).
  - <sup>3</sup> H.S. Goan and G.J. Milburn, Phys. Rev. B **64**, 235307 (2001).
  - <sup>4</sup> D.V. Averin, in: "Exploring the quantum/classical frontier: recent advances in macroscopic quantum phenomena", Ed. by J.R. Friedman and S. Han, (Nova Science Publishes, NY, 2003), p. 447; cond-mat/0004364.
  - <sup>5</sup> L. N. Bulaevskii and G. Ortíz, Phys. Rev. Lett. **90**, 040401 (2003).
  - <sup>6</sup> A. Shnirman, D. Mozyrsky, I. Martin, cond-mat/0311325.
  - <sup>7</sup> E. Il'ichev, N. Oukhanski, A. Izmalkov, Th. Wagner, M. Grajcar, H.-G. Meyer, A.Yu. Smirnov, A.M. van den Brink, M.H.S. Amin, and A.M. Zagorskin, Phys. Rev. Lett. **91**, 097906 (2003).
  - <sup>8</sup> D.V. Averin and R. Fazio, JETP Lett. **78**, 1162 (2003).
  - <sup>9</sup> W. Mao, D.V. Averin, R. Ruskov, and A.N. Korotkov, Phys. Rev. Lett. **93**, 056803 (2004).
  - <sup>10</sup> Yu. A. Pashkin, T. Yamamoto, O. Astafiev, Y. Nakamura, D.V. Averin, and J.S. Tsai, Nature **421**, 823 (2003).
  - <sup>11</sup> A.J. Berkley, H.Xu, R.C. Ramos, M.A. Gubrud, F.W. Strauch, P.R. Johnson, J.R. Anderson, A.J. Dragt, C.J. Lobb, and F.C. Wellstood, Science **300**, 1548 (2003).
  - <sup>12</sup> T. Yamamoto, Yu. A. Pashkin, O. Astafiev, Y. Nakamura, and J.S. Tsai, Nature **425**, 941 (2003).

- <sup>13</sup> J.B. Majer, F.G. Paauw, A.C.J. ter Haar, C.J.P.M. Harman, J.E. Mooij, cond-mat/0308192.
- <sup>14</sup> A. Izmalkov, M. Grajcar, E. Il'ichev, Th. Wagner, H.-G. Meyer, A.Yu. Smirnov, M.H.S. Amin, A.M. van den Brink, A.M. Zagorskin, Phys. Rev. Lett. **93**, 037003 (2004).
- <sup>15</sup> M. Field, C.G. Smith, M. Pepper, D.A. Ritchie, J.E.F. Frost, G.A.C. Jones, and D.G. Hasko, Phys. Rev. Lett. **70**, 1311 (1993).
- <sup>16</sup> E. Buks, R. Schuster, M. Heiblum, D. Mahalu, V. Umansky, Nature **391**, 871 (1998).
- <sup>17</sup> J.M. Elzerman, R. Hanson, J.S. Greidanus, L.H. Willems van Beveren, S. De Franceschi, L.M.K. Vandersypen, S. Tarucha, and L. P. Kouwenhoven, Phys. Rev. B **67**, 161308 (2003).
- <sup>18</sup> T. Hayashi, T. Fujisawa, H.D. Cheong, Y.H. Jeong, and Y. Hirayama, Phys. Rev. Lett. **91**, 226804 (2003).
- <sup>19</sup> S.A. Gurvitz, Phys. Rev. B **56**, 15215 (1997).
- <sup>20</sup> I.L. Aleiner, N.S. Wingreen, and Y. Meir, Phys. Rev. Lett. **79**, 3740 (1997).
- <sup>21</sup> Y. Levinson, Europhys. Lett. **39**, 299 (1997).
- <sup>22</sup> L. Stodolsky, Phys. Rep. **320**, 51 (1999).
- <sup>23</sup> D.V. Averin and K.K. Likharev, J. Low Temp. Phys. **62**, 345 (1986).
- <sup>24</sup> Yu. Makhlin, G. Schön, and A. Shnirman, Phys. Rev. Lett. **85**, 4578 (2000).
- <sup>25</sup> M.H. Devoret and R.J. Schoelkopf, Nature **406**, 1039 (2000).
- <sup>26</sup> G. Johansson, A. Käck, and G. Wendin, Phys. Rev. Lett. **88**, 046802 (2002).
- <sup>27</sup> A.B. Zorin, Phys. Rev. Lett. **76**, 4408 (1996).
- <sup>28</sup> A.A. Clerk, S.M. Girvin, A.K. Nguyen, and A.D. Stone, Phys. Rev. Lett. **89**, 176804 (2002).
- <sup>29</sup> J. Delahaye, J. Hassel, R. Lindell, M. Sillanpää, M. Paalonen, H. Seppä, and P. Hakonen, Science **299**, 1045 (2003).
- <sup>30</sup> O. Buisson, F. Balestro, J.P. Pekola, and F.W.J. Hekking, Phys. Rev. Lett. **90**, 238304 (2003).
- <sup>31</sup> S. Pilgram and M. Büttiker, Phys. Rev. Lett. **89**, 200401 (2002).
- <sup>32</sup> A.A. Clerk, S.M. Girvin, and A.D. Stone, Phys. Rev. B **67**, 165324 (2003).
- <sup>33</sup> D.V. Averin, Yu.V. Nazarov, and A.A. Odintsov, Physica B **165&166**, 945 (1990); G.-L. Ingold and Yu.V. Nazarov, in: *"Single Charge Tunneling"*, ed. by H. Grabert and M.H. Devoret (Plenum, New York, 1992), p. 21.
- <sup>34</sup> For measurements of other systems (different from the two qubits) expansion in the measured operators similar to Eq. (13) can be justified as the Taylor's expansion in weak detector-system coupling. Higher-order terms in this expansion should manifest themselves in measurements of larger number of qubits.
- <sup>35</sup> K. Blum, *Density matrix theory and applications*, (Plenum, NY, 1981).
- <sup>36</sup> R. Ruskov and A.N. Korotkov Phys. Rev. B **67**, 241305 (2003).
- <sup>37</sup> K. Rabenstein and D.V. Averin, Turk. J. Phys. **27**, 313 (2003); cond-mat/0310193.